Comparative study of dynamic characteristics between a FHAWT and a helical type FVAWT

Wanru Deng[1,2], Liqin Liu[1,*], Zihe Lin[1], Zhiming Yuan[2], Yan Li[1], Dongsheng Liu[1], Haoran Li[1], Ying Guo[3]

1 State Key Laboratory of Hydraulic Engineering Intelligent Construction and Operation, Tianjin University, Tianjin, 300072, China

2 Naval Architecture, Ocean and Marine Engineering Department, University of Strathclyde, Glasgow, United Kingdom

3 Tianjin Navigation Instrument Research Institute, Tianjin, 300131, China

*Corresponding author.
E-mail addresses: liuliqin@tju.edu.cn (Liqin Liu).

Abstract

Floating offshore wind turbines (FOWTs) are a growing area of interest, with significant ongoing research work and commercial development. There are two types of FOWT, namely floating horizontal axis wind turbine (FHAWT) and floating vertical axis wind turbine (FVAWT). It has been a long-standing debate on which type of FOWT has better technical and economic performance. However, the research work on comparative study of these two types of FOWT is very rare. In this study, we aim to systematically evaluate the performance of FHAWT and FVAWT, with particular focus on comparing their dynamic characteristics by using coupled numerical models. Tank testing for these two types of FOWT was conducted at the wave basin, and a series of code-to-experiment comparisons were carried out to validate the numerical models. Afterwards, dynamic characteristics, including the control strategy, aerodynamic power, floater motions, tower base bending moments, and blade deformations, are compared between the FHAWT and helical type FVAWT. Results show that the FHAWT presents better performance on the aerodynamic performance and tower base bending moments, while the helical type FVAWT has the advantage of minimal blade deformations.

Keywords: floating wind turbines, horizontal axis wind turbine, helical type wind turbine, comparative study, dynamic analysis

1. Introduction

Offshore floating wind farms are emerging as a viable solution for renewable energy generation as the corresponding technology continues to advance. Several commercial projects have been launched, such as Hywind in Norway (Hanson et al., 2011), WindFloat in Portugal (Roddier et al., 2010), Hywind Scotland in UK (Equinor, 2019), as well as CTGR (China Three Gorges Renewables) Yangjiang and CSIC (China Shipbuilding Industry Corporation) Zhanjiang in China (Zhang et al., 2022). Most of these projects deployed floating horizontal axis wind turbines (FHAWTs), and the dynamic characteristics of FHAWTs have been systematically studied in various

aspects, such as coupled numerical codes (Garrad Hassan, 2012; Jonkman et al., 2005; Nielsen et al., 2006), scaled model tests (Goupee et al., 2012; Cao et al., 2020), and dynamic response analysis (Li et al., 2018; Qu et al., 2020; Chen et al., 2021; Li et al., 2023).

To overcome the significant obstacle of the levelized cost of energy (LCOE), offshore wind turbines are being designed larger, with increasing rotor diameters. For instance, the Vestas 4.2 MW wind turbine had a rotor diameter of 117 m (V117-4.2 MW™ at a glance, 2010). In 2017, a 9.5 MW wind turbine was launched with a rotor diameter of 164 m (The world's most powerful available wind turbine gets major power boost, 2017). However, vibrations in the slender blades of large wind turbines can cause severe structural fatigue under harsh offshore wind environments. This issue could be worse for a floating wind turbine because the platform moves under both wind and wave loads simultaneously (Li et al., 2024a, Li et al., 2024b). Moreover, the nacelle needs to be designed larger and heavier owing to the longer blades, raising the center of gravity of the entire system. This is an unfavorable trend due to the acceleration sensitivity of the equipment installed in the nacelle (Leonardo et al., 2008).

In recent years, floating vertical axis wind turbines (FVAWTs) have gained growing attention as an alternative to supersized floating wind turbines (Jing et al., 2019, Kuang et al., 2022, Zhang et al., 2024). Various FVAWT concepts have been proposed, such as VertiWind (Cahay et al., 2011), DeepWind (Paulsen et al., 2015), SeaTwirl (SeaTwirl AB, 2024), and SKWID (Nakamura et al., 2013). Compared to FHAWTs, FVAWTs have a lower center of gravity because their generators are installed at the bottom of the wind turbine. This leads to lower installation and maintenance costs (Jing et al., 2019). Additionally, the rotational axis of FVAWTs is perpendicular to the wind direction, allowing it suitable for any wind direction without the utilization of a yaw control system. Furthermore, some researchers have found that the total power generation of closely arranged vertical axis wind turbines exceeds the sum of isolated ones, which could benefit the development of floating wind farms (Simone et al., 2015; Hansen et al., 2021; Jiang et al., 2022).

However, megawatt-scale FVAWTs are currently in the concept design stage,

and the technology is far from maturity. Straight-bladed or H-type VAWTs are significant types of vertical axis wind turbines due to the high level of average torque. However, straight-bladed VAWTs have several drawbacks, such as poor starting ability and significant oscillation of aerodynamic torque. To optimize traditional straight-bladed VAWTs, a helical type VAWT was designed. Battisti et al. (2016) compared the aerodynamic loads of straight and helical blade VAWTs, and the results showed that the twisted blade geometry of the helical blade VAWT could average and smooth out the cyclic oscillation of aerodynamic loads because different sections along the blade have a different angle of attack. Guo et al. (2019) calculated the effect of helical twist angle on the aerodynamic characteristics of a 5 MW helical type VAWT based on the double-multiple-stream tube theory and the Computational Fluid Dynamics method, and suggested an optimal helical twist angle ranging from 70° to 110°. Li et al. (2022) investigated a rotational speed control strategy for a 5 MW helical type FVAWT to provide the stable power output under different conditions. Deng et al. (2022a) developed a coupled numerical code to evaluate the dynamic responses of helical type FVAWTs. Based on this numerical code, the aerodynamic performance and blade dynamic characteristics were analyzed under various helical twist angles (Deng et al., 2022b). Results showed that helical twist angles ranging from 90° to 120° could significantly reduce aerodynamic torque fluctuations and suppress blade deformations. However, it should be noted that manufacturing helical blades is more challenging compared to straight blades, which may restrain the development of helical type FVAWTs to some extent.

Considering the current state of floating wind turbines described above, a comparison between FHAWTs and helical type FVAWTs is of vital importance. In recent years, several comparative studies have been conducted between FHAWTs and FVAWTs. Borg and Collu (2015) focused on the aerodynamic loads and their impact on the static and dynamic responses of the floating wind turbine. They compared several significant features, including thrust forces, static stability, and floating platform motions. Wang et al. (2014) modeled the FHAWT and FVAWT with a semi-submersible floating foundation, using the Simo-Riflex-Aerodyn code (Ormberg and

Bachynski, 2012) and the Simo-Riflex-DMS code (Wang et al., 2013), respectively. Time domain simulations were conducted under different scenarios, including decay tests, wave only conditions, wind only conditions, and combined wind and wave conditions. Cheng et al (2017a) proposed a control strategy for the FVAWT, and conducted coupled time domain simulations of the FHAWT and FVAWT. The generator power, tower base bending moments, and mooring tensions of the FVAWT presented prominent two-per-revolution variation due to the significant oscillation of aerodynamic loads. Cheng et al (2017b) further investigated the extreme structural responses and fatigue damage of the FHAWT and FVAWT.

The above studies provide valuable insights into the development of FVAWTs. Nonetheless, there are rare studies comparing the merits and drawbacks between the FHAWT and helical type FVAWT in literature. Moreover, blade deformation was not involved in the aforementioned studies. The blade deformation, as mentioned above, is of vital importance now that the floating wind turbines are being designed larger with an increasing rotor diameter. According to the NREL report (Stehly et al., 2019), capital expenditures of the turbine account for 24.4% of total financial costs, and the blade is a significant part. It is necessary to evaluate the dynamic responses of blades thus extending the long-term life of floating wind turbine systems.

In this point of view, this research aims to conduct a comparative study of the dynamic characteristics between the FHAWT and helical type FVAWT. Additionally, we lay an emphasis on the dynamic responses of the wind turbine blades. The remainder of this study is organized as follows. In section 2, the models of FHAWT and helical type FVAWT are introduced, along with the corresponding numerical code and theoretical basis. Section 3 validates the FHAWT and helical type FVAWT numerical models through a series of code-to-experiment comparisons. In section 4, the dynamic responses between the FHAWT and helical type FVAWT are specifically analyzed, including the control strategy, aerodynamic power, floater motions, tower base bending moments, and blade deformations. Ultimately, the conclusions are presented in the last section.

2. Methodology

2.1 Physical models

Fig. 1 shows a schematic of the helical type FVAWT and FHAWT investigated in this research. The FHAWT utilizes the OC4 semi-submersible floating foundation (Robertson et al., 2012) to support the NREL 5MW wind turbine (Jonkman et al., 2009). Similarly, the helical type FVAWT employs the same OC4 floating foundation. The OC4 semi-submersible floating foundation was initially designed for FHAWTs, so the ballast of the helical type FVAWT is adjusted to ensure the same draft as the FHAWT. The mooring system is also the same for both floating wind turbines. Three mooring lines are uniformly distributed with an interval of 120° to provide the restoring stiffness to the floater. The fairleads are located at the top of the base columns of the floating foundation and the anchors are located at a water depth of 200 m. Detailed parameters can refer to Robertson et al. (2012). Table 1 lists the main parameters of the wind turbine systems.

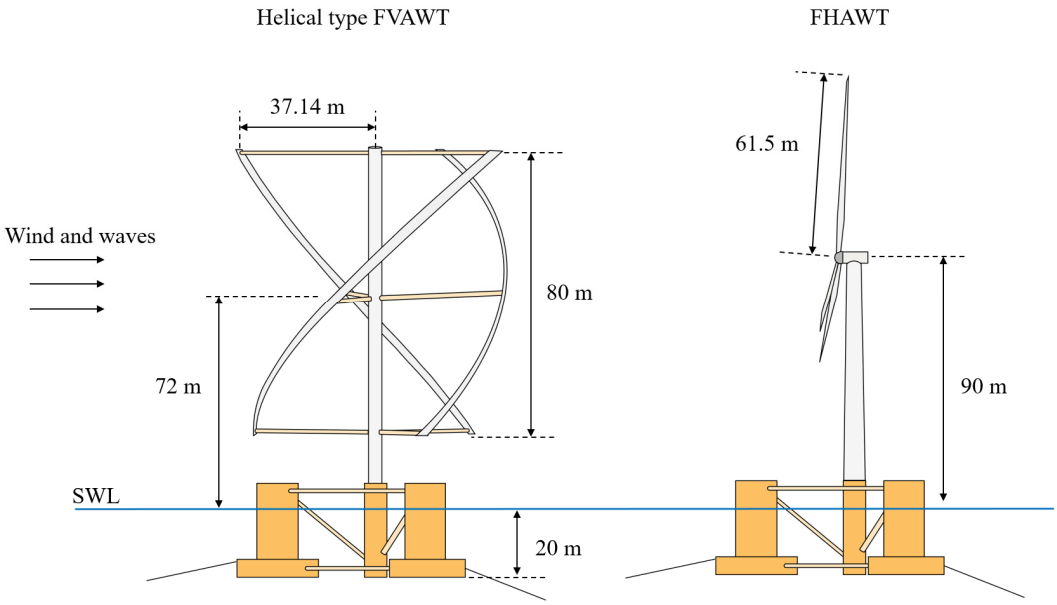

Fig. 1 Schematic of the helical type FVAWT and the FHAWT

Table 1 Main parameters of the wind turbine systems

Item	Helical type FVAWT	FHAWT
Water depth	200 m	200 m

Draft	20 m	20 m
Floating foundation mass (including ballast)	13576 t	13473 t
Center of gravity below still water level	10.75 m	9.88 m
Moment of inertia in roll direction	9.74×10^{9} kg·m^2	9.22×10^{9} kg·m^2
Moment of inertia in pitch direction	9.74×10^{9} kg·m^2	9.22×10^{9} kg·m^2
Moment of inertia in yaw direction	1.24×10^{10} kg·m^2	1.22×10^{10} kg·m^2

The helical wind turbine consists of three blades featuring a 120° helical twist angle, a tower, and three groups totaling nine struts. Parameters of the blade refer to a 5MW helical type wind turbine designed by Li et al. (2022). Table 2 provides the specifications of both wind turbines. It should be noted that the generator of the helical type FVAWT is mounted at the bottom of the tower, and the wind turbine mass includes only the masses of the blades, tower, and struts.

Table 2 Specifications of the wind turbines

Item	Helical type FVAWT	FHAWT
Rated power	5 MW	5 MW
Rotor radius	37.14 m	63 m
Wind speed operation range	5 m/s-25 m/s	3 m/s-25 m/s
Rated wind speed	14 m/s	11.4 m/s
Rated rotor speed	10.31 rpm	12.1 rpm
Blade number	3	3
Blade length	80 m (vertical direction)	61.5 m
Blade chord length	2.9 m	1.419 m-4.652 m
Blade mass	12039 kg	17740 kg
Tower length	102 m	77.6 m
Tower mass	398450 kg	249718 kg
Wind turbine mass	496980 kg	599718 kg

2.2 Coupled numerical method

The dynamic response calculation of a floating wind turbine is a multi-disciplinary research field that involves aerodynamics, hydrodynamics, control dynamics, structural

dynamics, etc. Given the complexity of these interactions, nonlinear coupled simulation tools are essential for studying the dynamic behaviors. For the case of the FHAWT, commercial software SESAM/Sima (SIMO 4.14.0 User Guide, 2018; RIFLEX 4.14.0 User Guide, 2018) was employed. SESAM/Sima is a simulation tool that integrates aerodynamics, hydrodynamics, and structural dynamics for floating wind turbines. The hydrodynamic loads are calculated using potential flow theory and/or Morison's equation. The structural dynamics of flexible bodies, such as blades, are typically modeled using the beam element method. Fig. 2 presents the FHAWT model that was created in Sima.

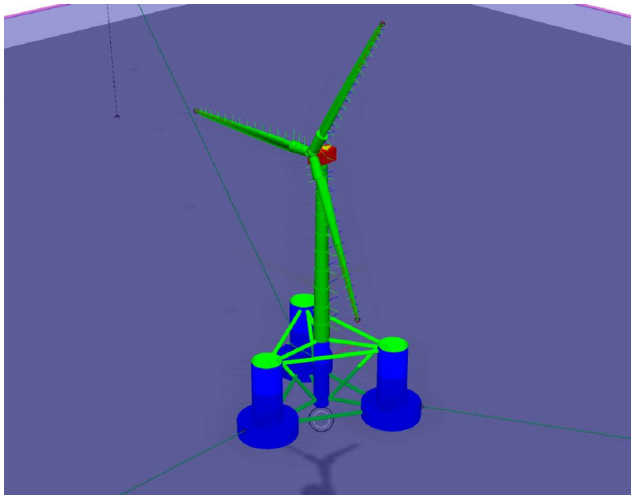

Fig. 2 FHAWT model in SIMA

For the dynamic analysis of the helical type FVAWT, some numerical codes have been developed for internal use, such as FloVAWT (Borg and Collu, 2015), Simo-Riflex-DMS (Wang et al., 2013), and Simo-Riflex-AC (Cheng et al., 2017a), but there is still no publicly available tool specifically designed for the dynamic calculation of FVAWTs. Therefore, we modeled the helical type FVAWT using our in-house numerical code. The code was originally developed for simulating straight-bladed FVAWTs (Deng et al., 2018; Deng et al., 2020). We later added a helical blade module to simulate the dynamic response of the helical type FVAWT. In this subsection, the code is briefly elaborated. More details could be found in Deng et al. (2022a).

The helical type FVAWT system consists of several components, including the floating foundation, mooring system, tower, blades and struts. In the numerical code,

the floating foundation is considered as a rigid body with six degrees of freedom (DOFs): surge, sway, heave, roll, pitch, and yaw. The tower and blades are modeled as Euler–Bernoulli beams using the continuum mechanics theory and finite element method. For the external loads, restoring forces of the mooring lines are obtained using the quasi-static catenary method (Ractliffe, 1985). Wave loads are derived from the SESAM/Wadam software. Aerodynamic loads are calculated using the UBEM (Unsteady Blade Element Momentum) theory considering time-delay effects caused by dynamic wakes or dynamic inflows (Bangga et al., 2020). Using momentum theory, the induction factor of the blade can be derived from momentum loss and rotor thrust, with the induction factors converging over time. Throughout this process, the aerodynamic loads of the wind turbine can be determined. A series of aero-dynamic corrections was considered, including B-L dynamic stall model, Prandtl's tip-loss theory, and dynamic inflow correction (Deng et al., 2024). These external loads are incorporated into the wind turbine system at each time step to enable the coupling between the structure and loads. Furthermore, a variable speed control strategy is applied to regulate the rotational speed of the rotor considering that the blade pitch control is not suitable for the helical blade wind turbine (Li et al., 2022). This control strategy ensures rapid adjustment of the wind turbine to maximize the power capture in low wind speeds and maintains stable power output in high wind speeds. The PID-based control algorithm is shown in Fig. 3. Notably, when modeling the wind turbine, we used a slack coupled method by decomposing the system into two configurations that are coupled based on aerodynamic loads and large overall motions of the blades (Deng et al., 2022a). By using this method, the accuracy of the dynamic response of the wind turbine system could be maintained and the results could be solved faster. Fig. 4 illustrates the calculation flowchart of the in-house numerical code.

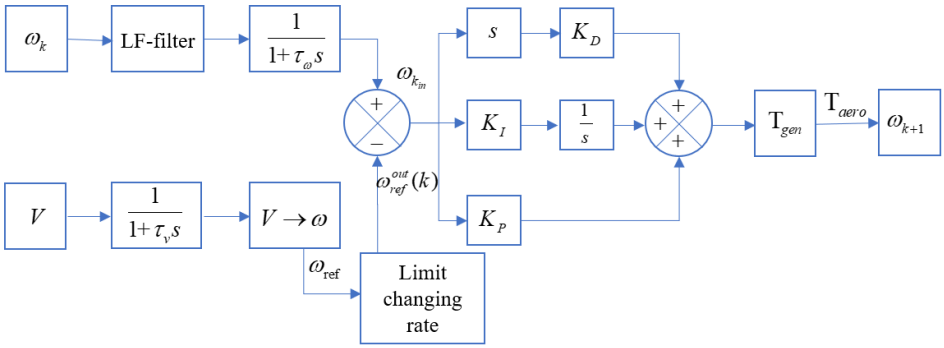

Fig. 3 PID-based rotational speed controller (Li et al., 2022)

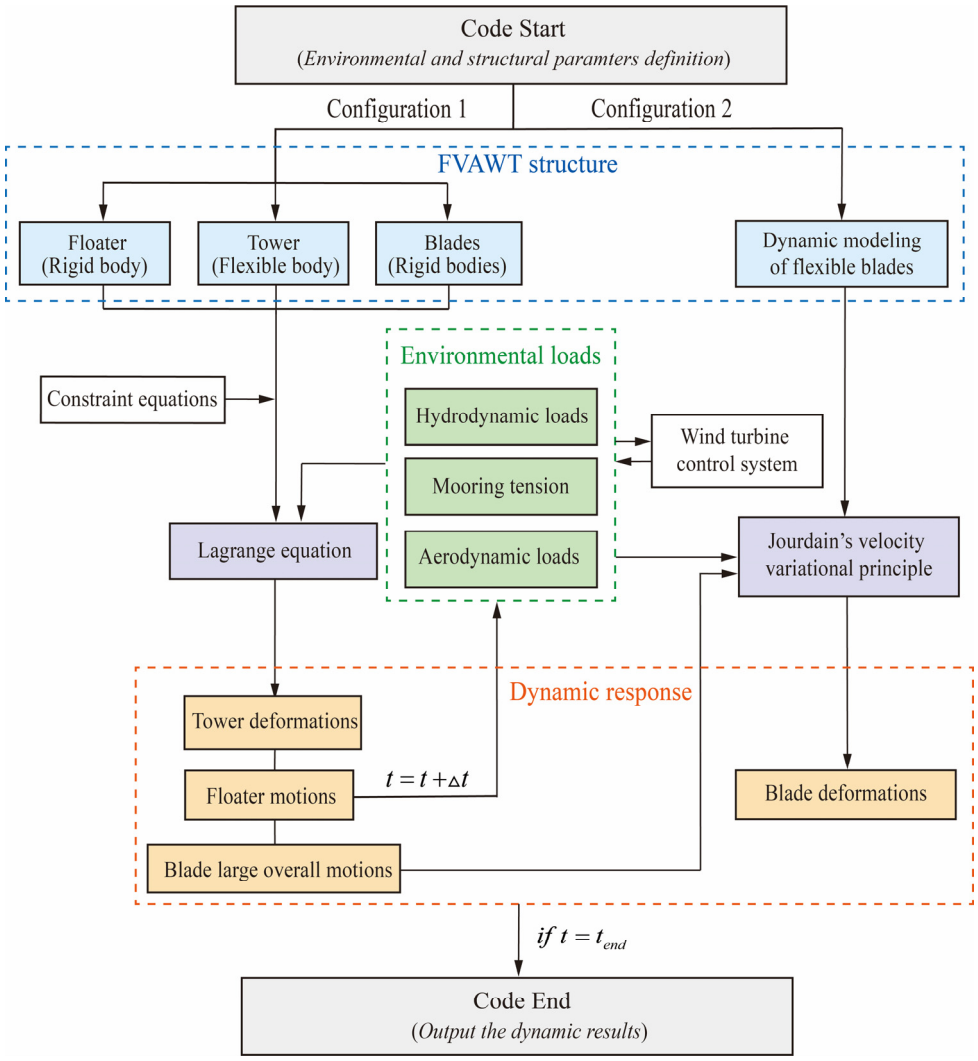

Fig. 4 Calculation flowchart of the in-house numerical code

3. Numerical Model Validation

As presented previously, the helical type FVAWT was simulated based on our in-house numerical code, and the FHAWT was modeled based on the commercial software

SESAM. Before the comparison, it is necessary to test the feasibility of the numerical models. In this section, the models will be validated through a series of code-to-experiment comparisons.

3.1 Validation of the numerical model of the Helical type FVAWT

In our previous studies, validation work for the helical type FVAWT was conducted (Deng et al., 2022a; Deng et al., 2022b). Floater motions calculated by the numerical code were validated in comparison with a single rigid body code (Liu et al., 2017). In addition, blade deformations and natural frequencies were validated by using the finite element analysis software ANSYS. To conduct a further validation, a helical type floating wind turbine model test is introduced in this subsection. The free decay test and the combined wind and wave test are presented for the comparison process.

The model test was carried out in the towing wave tank at Tianjin University, as shown in Fig. 5. The physical model was fabricated based on the 1/50 Froude-scaled rule, while the Reynolds number similarity was neglected. The model consisted of a helical type wind turbine with three blades mounted on an OC4 semi-submersible floating foundation. The model blades and the prototype blades satisfy the geometric scaling ratio. Carbon fiber epoxy composite material was used to manufacture the blades. Tracking markers were installed on one of the offset columns to measure the floater motions. Tensile force sensors were placed near the fairleads to measure the forces on the mooring lines. The blade-pitch controller is not suitable for the helical type FVAWT due to its structural characteristics. A speed sensor was designed to actively monitor the rotational speed of the wind turbine. When a steady wind was generated, the rotor speed did not change during the test. More details on the experimental setup and results could be found in Deng et al. (2023).

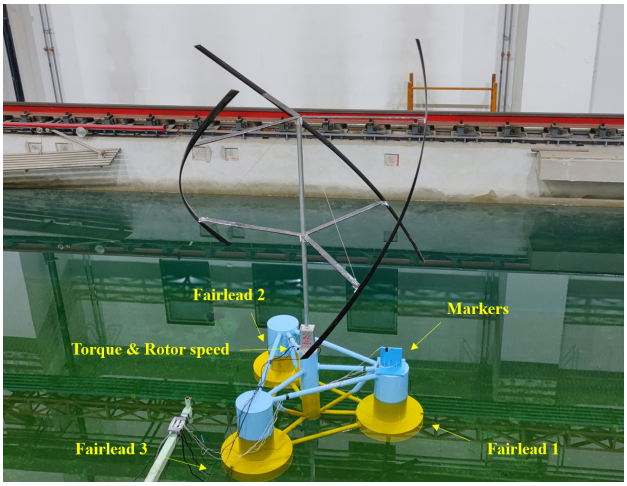

Fig. 5 Helical type FVAWT model in the wave basin

Fig. 6 illustrates the layout of the floating wind turbine system during the experiment. The wind array system and the wave generating system were positioned on the right side of the wave basin. The wind array system consisted of 10 controllable axial fans in a 2×5 rectangle configuration. The generated wind and waves were aligned with the surge direction of the floating foundation. Before the wind turbine experiment, some identification tests were conducted. The wind field and wave elevations were measured to ensure the accuracy of environmental loads during the model test (Deng et al., 2023).

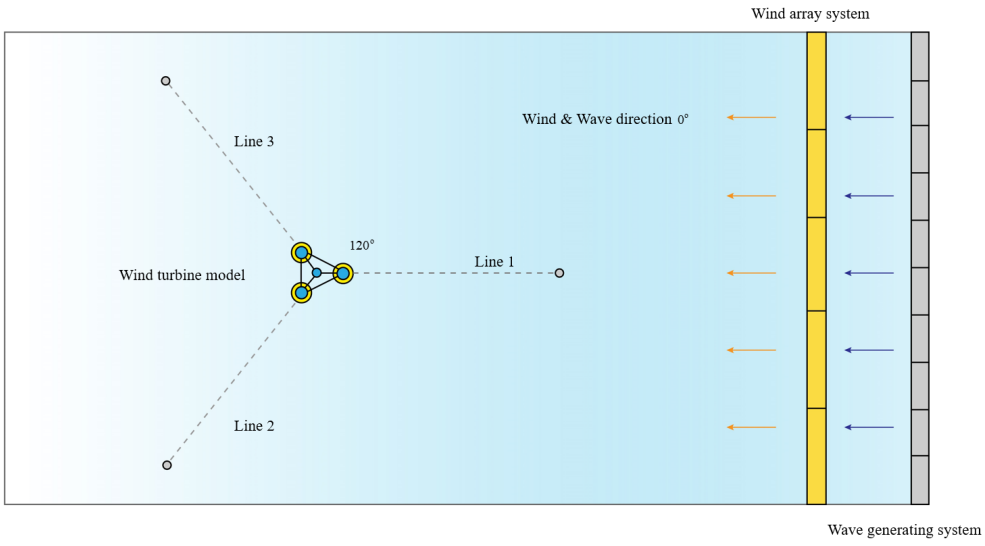

Fig. 6 Top view of the wave basin

The parameters of the numerical model were kept the same as the physical model, as given in Tables 1 and 2. The only difference between the numerical and experimental model is the arrangement of the struts. However, it was assumed that this difference would only slightly affect the wind field and have little effect on the dynamic responses of the wind turbine.

A free decay test was first conducted to validate the accuracy of the numerical code, which involves observing the motion of the floating wind turbine after it is released from an initial displacement. Fig. 7 shows the results for surge, heave, and pitch motions, and the natural periods of these motions are compared in Table 3. The natural period indicates the time taken for the floating wind turbine to complete one cycle of motion in each DOF. Hydrodynamic damping coefficients utilized in the numerical simulation were derived from the model test. Overall, the experimental and numerical results match well, with a small discrepancy in the surge motion. The discrepancy could potentially be attributed to a stiffness error in the mooring lines, affecting the restoring force acting on the wind turbine during the experimental process. The mooring lines were fabricated using the truncation method (Molins et al., 2015) due to the dimension restriction of the wave basin, which may lead to a slight stiffness error.

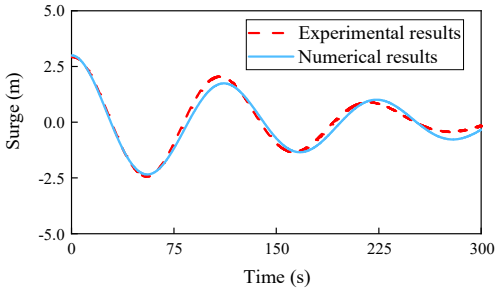

(a) Surge

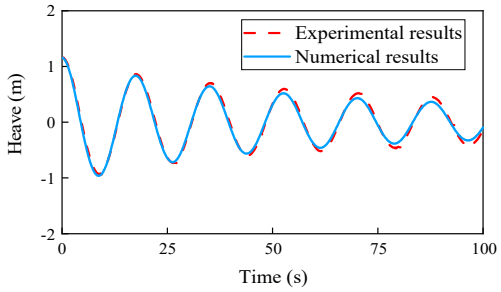

(b) Heave

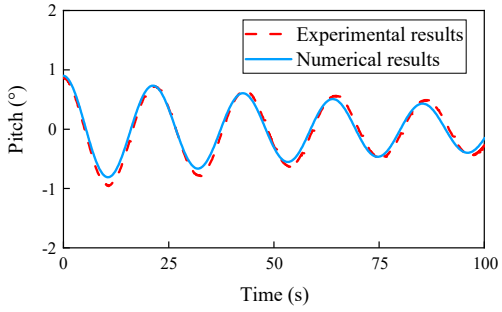

(c) Pitch

Fig. 7 Time histories of the helical type FVAWT under free decay test

Table 3 Natural period comparison results of the helical type FVAWT

DOF	Experimental results (s)	Numerical results (s)
Surge	103.6	113.5
Heave	17.6	17.8
Pitch	21.4	21.7

A combined wind and wave test was adopted to further conduct the comparative study, with steady wind and irregular waves directed along the surge motion. The wind speed was 14 m/s. Irregular waves were generated by applying the JONSWAP spectrum, with a significant wave height of 3.62 m and a spectral peak period of 10.29 s. Time series of dynamic responses were derived, and Fourier transform was applied to obtain the power spectra. Fig. 8 shows a comparison of the power spectra results of the floater motions and restoring force on mooring line 1, which directs along the surge direction. The floater motions mainly comprise the wave frequency and its natural frequency components. A small surge frequency component appears in pitch motion, showing the coupled behavior between surge and pitch motions (Duan et al., 2016).

Table 4 compares the standard deviations of dynamic responses. The standard deviation in surge motion has an error of 25.9%, which is significantly larger than that in heave motion. This discrepancy is primarily due to the horizontal orientation of surge motion, making it more sensitive to aerodynamic loads compared to the vertical heave motion. The neglect of Reynolds number similarity in the model test contributed to errors in the aerodynamic loads, resulting in a larger error in the standard deviation of surge motion.

Although surge and pitch motions are coupled, the standard deviation in pitch motion exhibits a small error of 3.0%. This is because the standard deviation of pitch motion is inherently small (less than 1°), making it more sensitive to other influencing

factors. For example, due to the restriction of the wave basin dimensions, the truncation method was utilized for the mooring lines, which may cause a stiffness error (Deng et al., 2023). Operational and measurement errors during the experimental process also inevitably affected the results. Furthermore, in the numerical simulation, potential theory was used for hydrodynamic calculations, which meant that the viscous effect of the fluid could not be accurately simulated.

In general, the numerical and experimental results show a good agreement, indicating that our numerical code is feasible for performing dynamic responses of the helical type FVAWT.

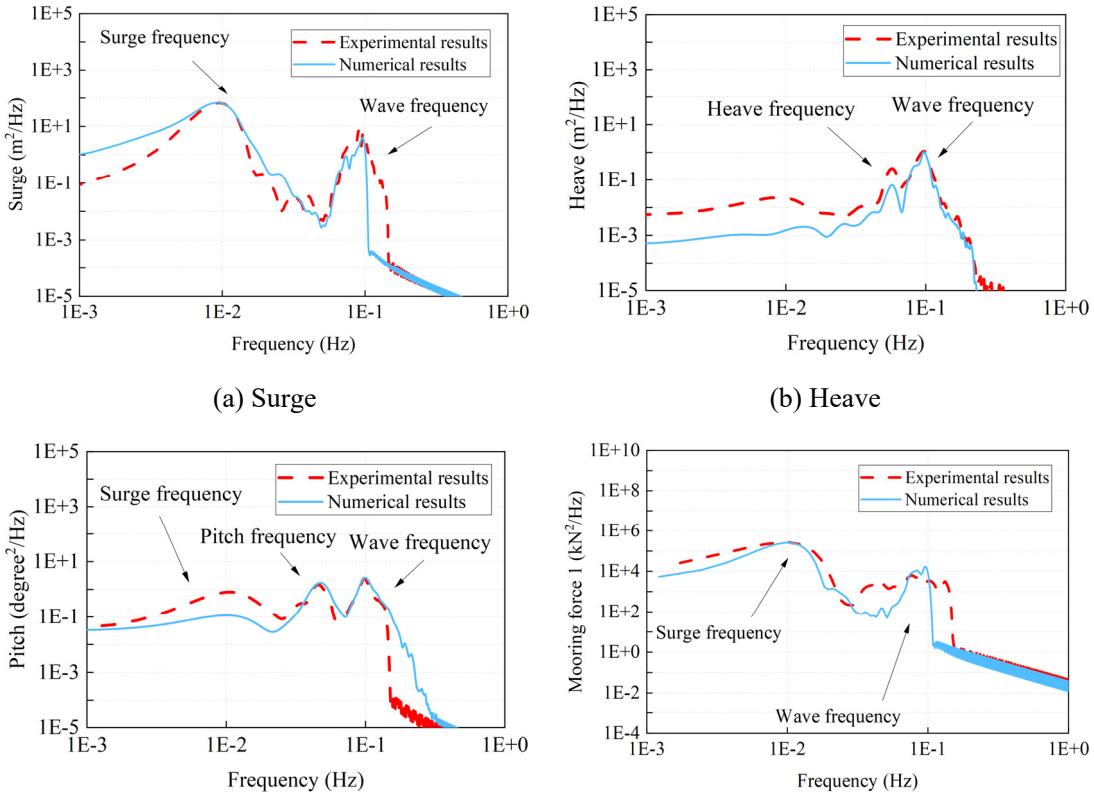

(a) Surge (b) Heave

(c) Pitch (d) Mooring line 1

Fig. 8 Power spectra of the helical type FVAWT under combined wind and wave test

Table 4 Standard deviation comparison of the helical type FVAWT

Item	Experimental results (a_1)	Numerical results (a_2)	Percentage error $\left(\left\|\frac{a_1-a_2}{a_1}\right\|\times 100\%\right)$
Surge	0.58 m	0.43 m	25.9%

Heave	0.16 m	0.18 m	12.5%
Pitch	0.33 °	0.32 °	3.0%
Mooring line 1 force	3.93×10^4 N	3.31×10^4 N	15.8%

3.2 Validation of the numerical model of the FHAWT

Fig. 9 shows the FHAWT experimental model, which was also tested in the towing wave tank at Tianjin University. The model consisted of the NREL 5MW wind turbine and the OC4 semi-submersible floating foundation. The parameters of the physical model obeyed the 1/50 Froude-scaled rule compared with the prototype numerical model. The free decay test and the combined wind and wave test are presented for the comparison of the experimental model and numerical model. The experimental process was similar to that of the helical type FVAWT, as introduced in subsection 3.1. Note that the blade pitch control was not considered in the model test.

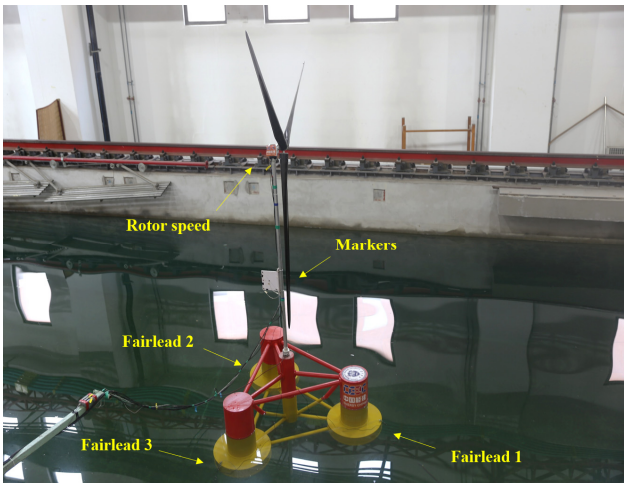

Fig. 9 FHAWT model in the wave basin

Fig. 10 shows the results of the free decay test for surge, heave, and pitch motions, and the natural periods are compared in Table 5. The results show that there is a good agreement within the range.

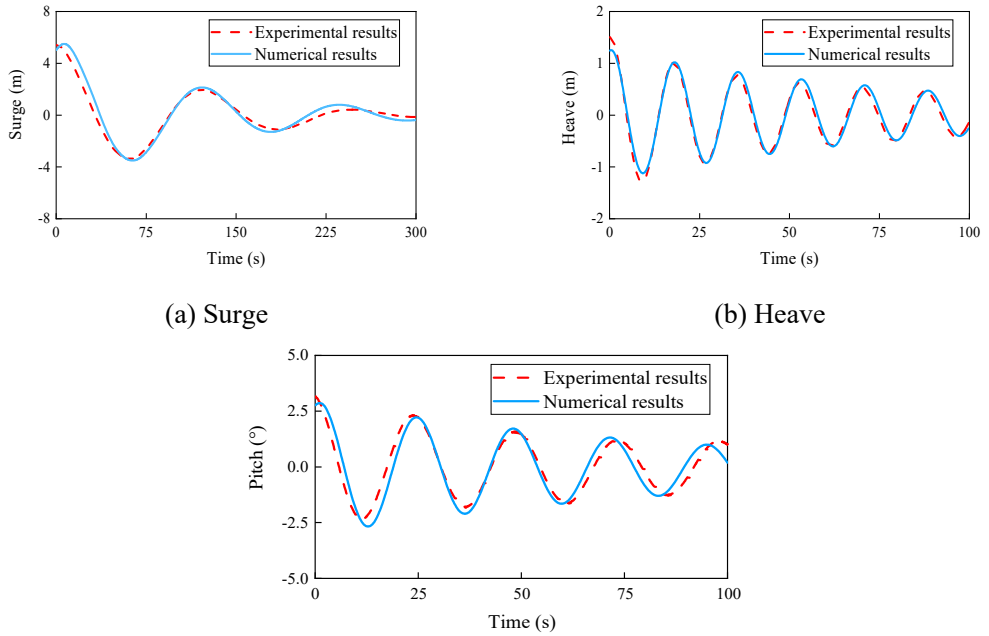

(a) Surge (b) Heave

(c) Pitch

Fig. 10 Time histories of the FHAWT under free decay test

Table 5 Natural period comparison results of the FHAWT

DOF	Experimental results (s)	Numerical results (s)
Surge	123.2	113.2
Heave	17.4	17.6
Pitch	23.6	21.3

The responses of the FHAWT experimental and numerical model for the combined wind and wave case is compared. The steady wind and irregular waves directed along the surge motion. The wind speed was 11.4 m/s, and irregular waves were generated by applying the JONSWAP spectrum with a significant wave height of 6m and a spectral peak period of 10 s. Fig. 11 shows the power spectra comparison results of the surge, heave, pitch motions, and restoring force on mooring line 1. Table 6 compares the standard deviations of dynamic responses. It can be concluded that the FHAWT numerical model established in SESAM software is feasible to predict the dynamic responses of the wind turbine. As listed in Table 6, the discrepancies between numerical and experimental results are similar to the FVAWT results discussed in Section 3.1.

However, the error in pitch motion is notably larger. This is because the standard deviation of pitch motion is very small, making it highly sensitive to various factors.

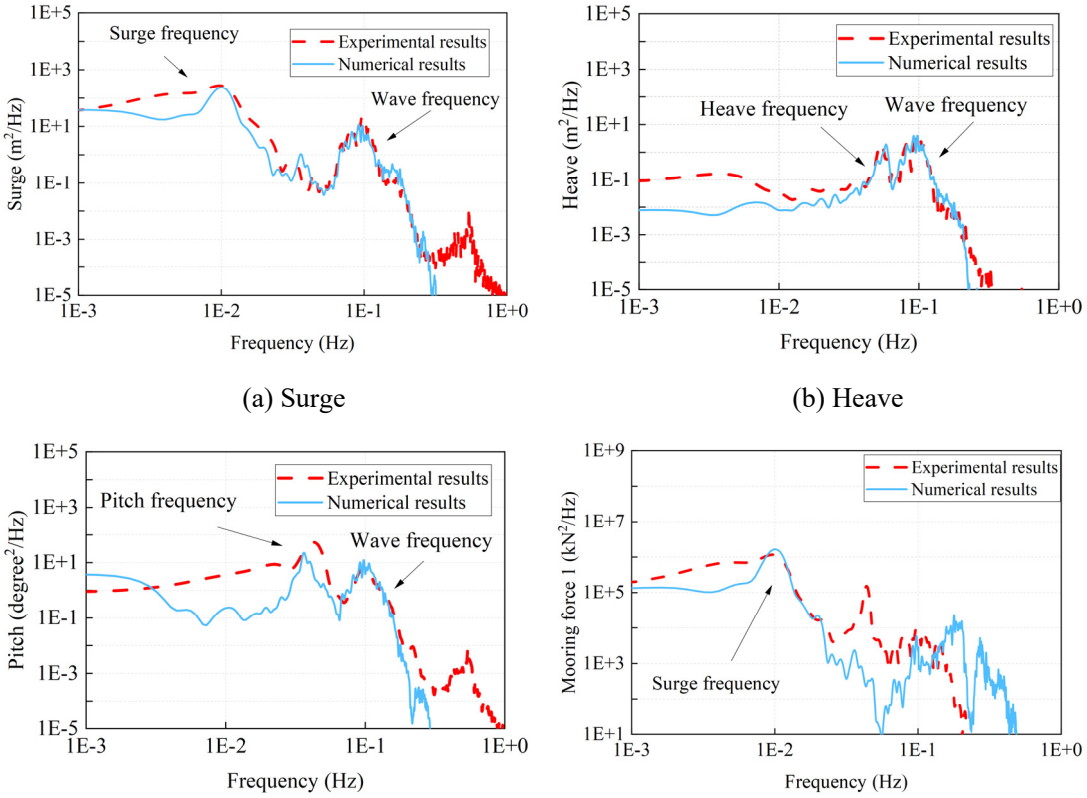

(a) Surge (b) Heave

(c) Pitch (d) Mooring line 1

Fig. 11 Power spectra of the FHAWT under combined wind and wave test

Table 6 Standard deviation comparison of the FHAWT

Item	Experimental results (b_1)	Numerical results (b_2)	Percentage error $\left(\left\|\frac{b_1-b_2}{b_1}\right\|\times 100\%\right)$
Surge	1.51 m	1.10 m	27.2%
Heave	0.31 m	0.29 m	6.5%
Pitch	0.69 °	0.51 °	26.1%
Mooring line 1 force	1.22×10^5 N	1.39×10^5 N	13.9%

4. Results and Discussion

4.1 Load cases

Table 7 lists three typical load cases simulated for the FHAWT and helical type FVAWT, representing the cut-in case (LC1), rated case (LC2), and cut-out case (LC3) of the helical type FVAWT. Environmental parameters refer to Cheng et al. (2017a), which were derived from the database from data collected in the northern North Sea (Johannessen et al., 2002). The constant wind and irregular waves are considered. The wind shear effect is included during the simulations. The irregular waves are generated by applying the JONSWAP spectrum. It is assumed that the directions of wind and waves coincide, which directs along the surge motion, as exhibited in Fig. 1. Dynamic responses of the wind turbine under the time series of 3600 s are processed after removing the initial part to eliminate the start-up transients. Unless specified otherwise, the VAWT and FVAWT mentioned in this section represent the helical type VAWT and helical type FVAWT, respectively.

Table 7 Parameters of the load cases

Case No.	Wind speed	Significant wave height	Spectral peak period
LC1	5 m/s	2.10 m	9.74 s
LC2	14 m/s	3.62 m	10.29 s
LC3	25 m/s	6.02 m	11.38 s

4.2 Aerodynamic behaviors

Fig. 12 compares the control strategies of two wind turbines, including the rotational speed and the corresponding power output at different wind speeds. The FHAWT operates within a wider wind speed range of 3 m/s to 25 m/s (from cut-in case to cut-out case) (Jonkman et al., 2009), whist the FVAWT has a narrower range of 5 m/s to 25 m/s due to its inferior self-starting performance. The rated wind speeds of the FHAWT and FVAWT are 11.4 m/s and 14 m/s respectively, as labeled in the figure.

The working range could be roughly separated into two regions based on the rated wind speed. Before the rated wind speed, a rotational speed control strategy is employed

for both wind turbines to achieve an optimum tip speed ratio (TSR) for maximizing power output. In this region, The FHAWT exhibits higher aerodynamic power. Additionally, for the FVAWT, there is a small region where the rotational speed exceeds the rated value while the wind speed is still lower than its corresponding rated speed. In this scenario, the rotational speed is maintained at the rated level to alleviate oscillating aerodynamic loads.

When the wind speed exceeds the rated value, the control strategy differs for the two wind turbines. For the FHAWT, the rotational speed remains at its nominal value, and the blade-pitch control module activates, aiming to stabilize power capture at approximately 5.3 MW. However, the blade-pitch controller is not suitable for the FVAWT owing to its structural characteristics. Thus, the rotational speed control module continues to work to achieve stable power output. In this region, the rotational speed decreases as the wind speed increases, and the slope depends on the rated aerodynamic power.

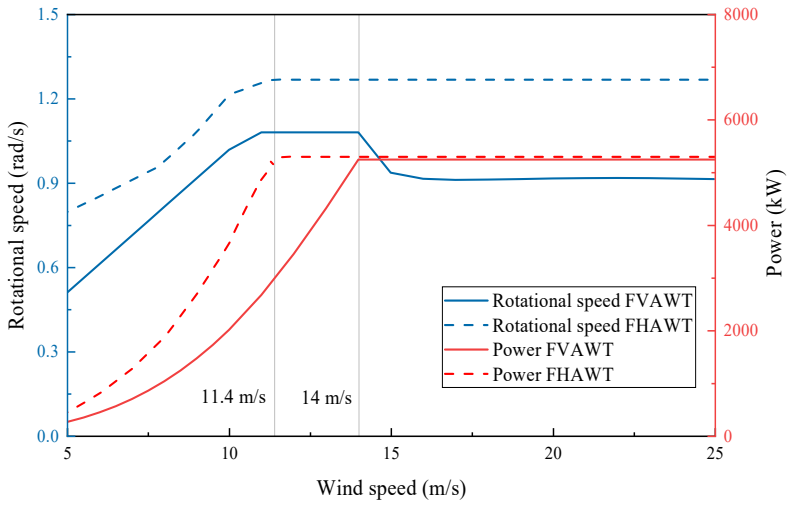

Fig. 12 The rotational speed and corresponding power output via different wind speeds

Fig. 13 compares the polar diagram of the aerodynamic power under three load cases. For clarity, the figure only shows data from the time series of 200 seconds. Under LC1, the wind speed is 5 m/s, so the FHAWT exhibits a larger power output owing to its higher power coefficient. As for LC2 and LC3, the average power output is similar, but the FVAWT presents stronger power fluctuations. This variability can be attributed

to two reasons. Firstly, the revolution azimuth angle of the blade varies periodically as the rotor rotates. This results in a large fluctuation of aerodynamic loads, as the lift and drag forces on each blade may reach their maximum values at the same time (Deng et al., 2023). The rotational frequency can be expressed as 1P, so that the aerodynamic power of the three-bladed FVAWT investigated in this research exhibits a 3P frequency characteristic, as obviously seen in Fig. 13(c). Secondly, differences in control strategies play a role. As mentioned above, the rotational speed controller employed in the FVAWT may be acknowledged as a less efficient strategy compared to the blade pitch controller employed in the FHAWT when the wind speed exceeds the rated value. Moreover, continuously changing the rotational speed may lead to fatigue issues, given that FVAWTs typically have long rotational shafts and towers (Hand and Cashman, 2020).

In summary, although the FVAWT model has a helical type wind turbine with three blades, which has a lower aerodynamic torque oscillation compared to a straight blade (Deng et al., 2022b) or two-blade design (Cheng et al., 2017c), it still exhibits inferior power output stability compared to the FHAWT.

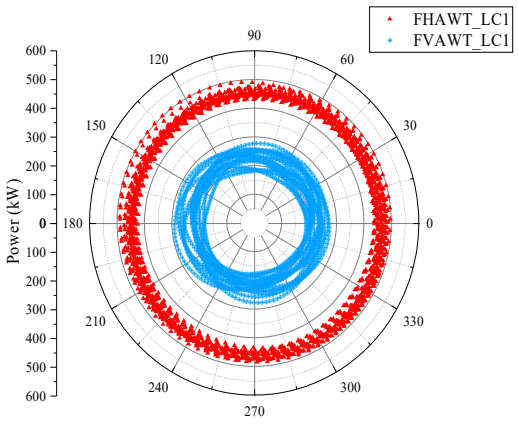

(a) LC1

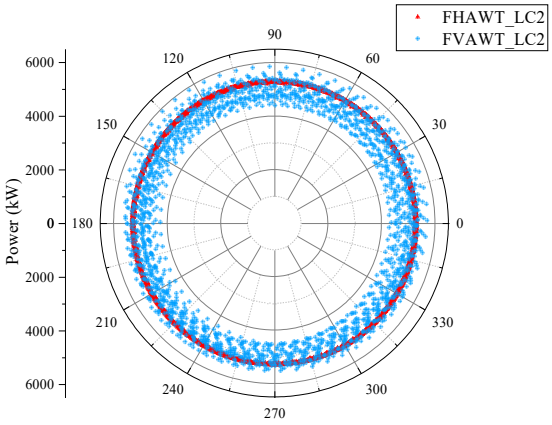

(b) LC2

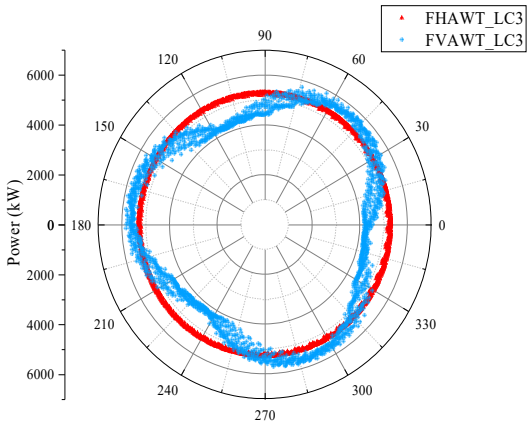

(c) LC3

Fig. 13 Polar diagram of aerodynamic power during the time series of 200s

4.3 Floater motions

Fig. 14 shows the mean values of floater motions. Sway and roll motions are negligible and not presented in the figure. In general, the mean values of the FVAWT are larger than those of the FHAWT, especially under high wind speed case. Mean values of floater motions are closely related to aerodynamic loads. For the surge motion, its mean value is positively correlated with the aerodynamic thrust. From LC1 to LC3, the mean value of the FVAWT increases with higher wind speeds. However, the maximum mean value of the FHAWT occurs under LC2, since the blade pitch controller engages to reduce the thrust when the wind speed exceeds the rated value. The results for pitch motion exhibit a similar trend to surge motion, reflecting their correlation.

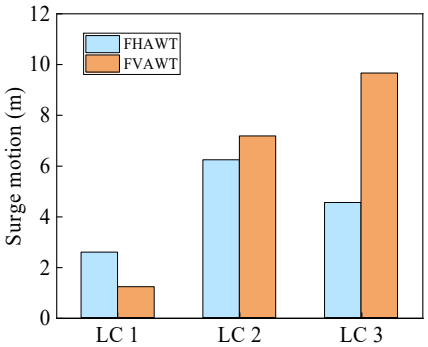

(a) Surge

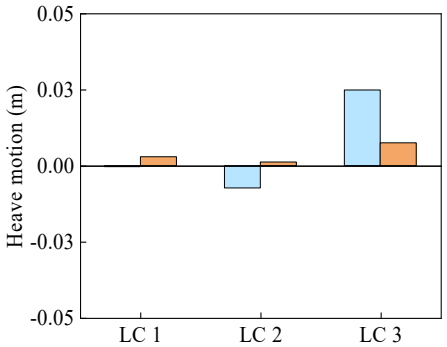

(b) Heave

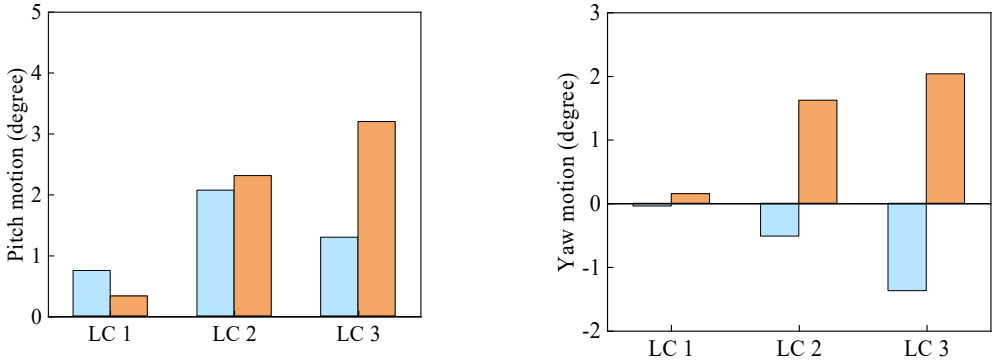

(c) Pitch (d) Yaw

Fig. 14 Average values of floater motions

Fig. 15 compares the standard deviations of floater motions, which are mainly driven by wave loads. With the same OC4 semi-submersible floating foundation and similar center of gravity location, the standard deviations of the two wind turbines in surge, heave, and pitch motions are similar. The main discrepancy lies in the yaw motion. The standard deviations of yaw motion of the FHAWT are minimal under all cases. In contrast, the yaw motion of the FVAWT exhibits larger fluctuations compared with that of the FHAWT. Moreover, it should be noted that the standard deviation of the FVAWT in yaw motion under LC2 is significantly larger than that under LC3, despite LC3 having a higher wind speed and more severe wave condition. This disparity may be due to the rotational speed control strategy employed by the FVAWT. As shown in Fig. 12, the blue solid line, which represents the rotational speed variation under different wind speeds, has a steeper gradient near 14 m/s while a shallower gradient near 25 m/s. Therefore, the rotational speed will alter rapidly when the wind speed is near its rated value. This may lead to the substantial oscillation of the torque, resulting in a larger fluctuation of the yaw motion under LC2.

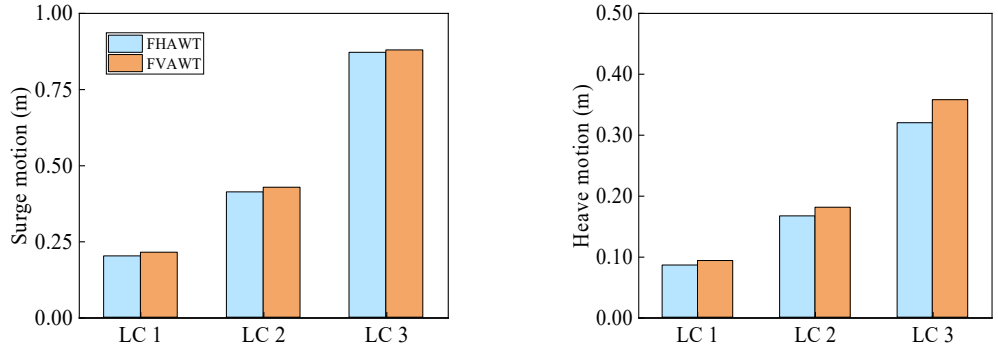

(a) Surge (b) Heave

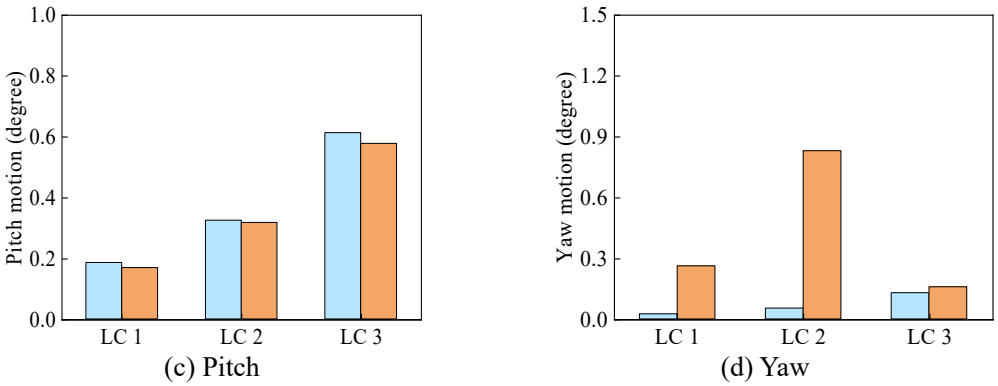

(c) Pitch (d) Yaw

Fig. 15 Standard deviations of floater motions

The amplitude spectra of floater motions are derived based on Fourier transform and shown in Fig. 16. The wave and natural frequencies could be obviously observed. Natural frequencies include surge, pitch, and yaw frequencies. In the numerical calculation, second order wave forces are taken into consideration. As a consequence, peaks of natural frequency components are motivated mainly by difference frequency wave forces. A low-frequency component labeled as “Control frequency” is also seen in Fig. 16(d), representing the variation frequency of the rotational speed controller of the FVAWT.

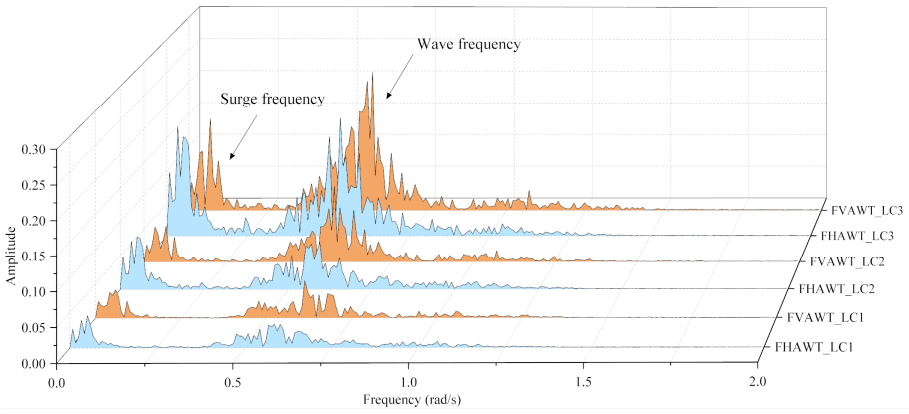

(a) Surge

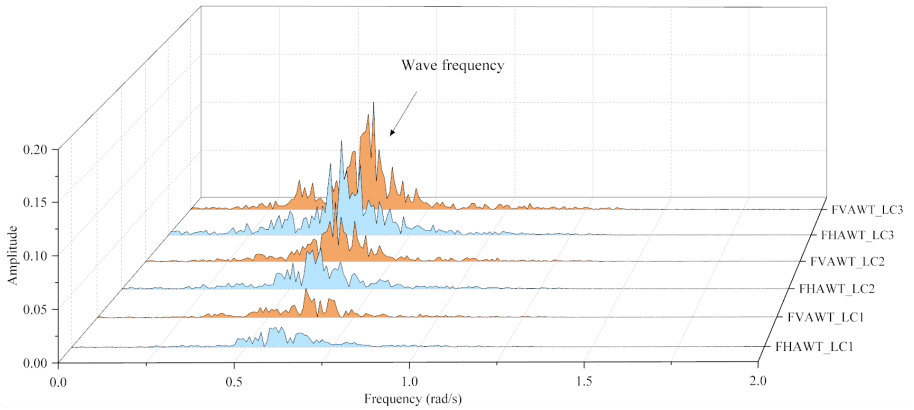

(b) Heave

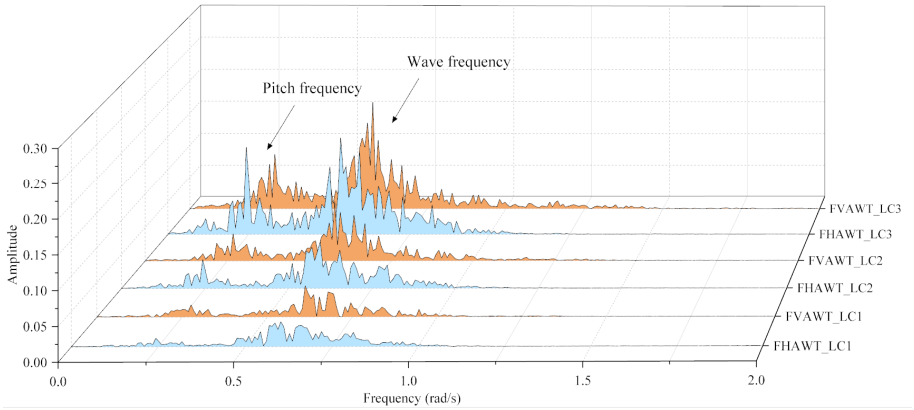

(c) Pitch

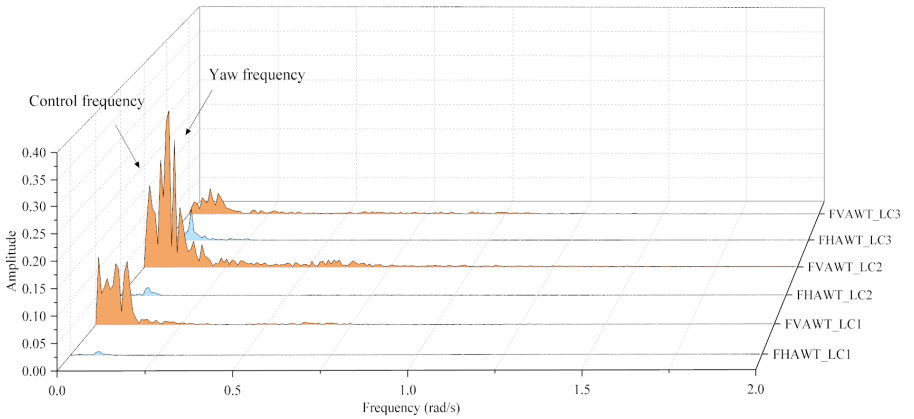

(d) Yaw

Fig. 16 Amplitude spectra of floater motions

4.4 Tower base bending moments

The tower is a critical component in a floating wind turbine system, mainly subjected to aerodynamic loads and inertia loads on the rotor. In addition, floater

motions can also influence bending moments on the tower. In this subsection, tower base bending moments are discussed.

Fig. 17 shows statistical results of the tower fore-aft bending moment (represented by "Mx") and side-to-side bending moment (represented by "My"). As previously mentioned, the direction of wind and waves is along the surge motion. Hence, the tower base bending moments on the two wind turbines are mainly induced by the fore-aft bending components rather than side-to-side bending components. Generally speaking, the FVAWT exhibits lower mean values of fore-aft bending moments compared to the FHAWT. However, the standard deviations of the FVAWT are significantly larger than those of the FHAWT. For instance, under LC3, the standard deviation of the FVAWT fore-aft bending moment is over twofold that of the FHAWT. Moreover, the maximum values of the FVAWT are also larger than those of the FHAWT under LC2 and LC3. This poses challenges for the fatigue damage issue of the wind turbine tower.

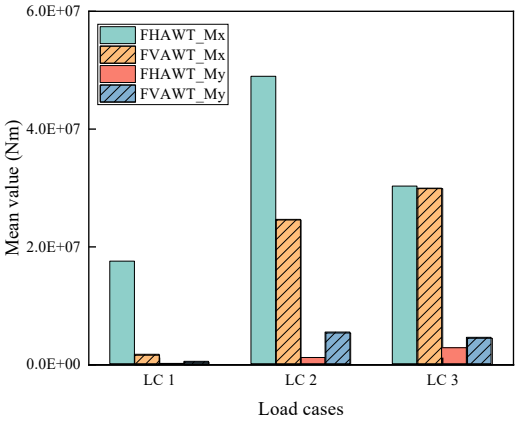

(a) Average value

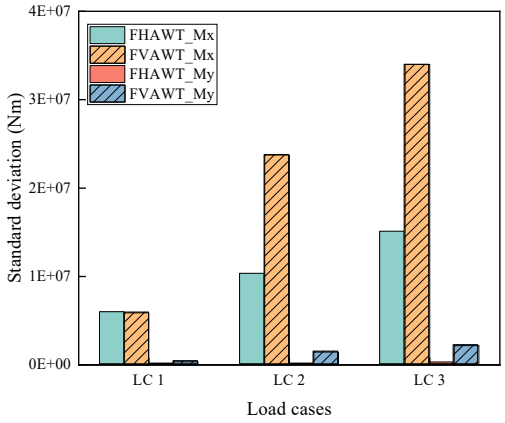

(b) Standard deviation

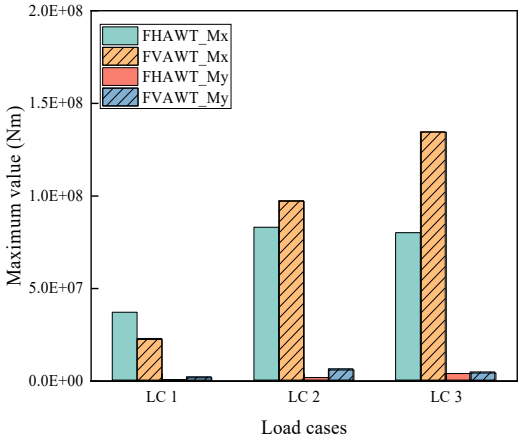

(c) Maximum value

Fig. 17 Statistical results of tower base bending moment

4.5 Blade deformations

When the wind turbine blades rotate, they encounter significant geometric effects and aeroelastic issues (Xu et al., 2020). For a floating wind turbine, changes in floater orientation alter aerodynamic loads, resulting in more complicated dynamic performance on the blades. Therefore, it is crucial to analyze the blade deformation under harsh environmental conditions in deep seas.

Fig. 18 compares statistical results of the blade deformation, including the average value, standard deviation, and maximum value. To provide a straightforward view, deformation trajectories of the blade deformations are also presented in Fig. 19. For the FHAWT, the leading edge of the blade is selected for analysis as it typically experiences the highest deformation at the blade tip. The flapwise deformation (labeled as FHAWT_flapwise) shown in Fig. 18 directs out of the rotor plane, while the edgewise deformation (labeled as FHAWT_edgewise) directs in the rotor plane. Regarding the FVAWT, the helical blade is segmented into 12 elements based on the finite element method. Our previous study (Deng et al., 2022b) investigated the same type of helical blade, it was found that when the blade is divided into 12 elements, the deformation on node 9 normally has the maximum value. Therefore, deformation on node 9 of the helical blade is selected for comparison. The tangential deformation (labeled as FVAWT_flapwise) is along the chord length direction, while the edgewise deformation (labeled as FVAWT_edgewise) is perpendicular to the tangential deformation.

The blade deformations of the FVAWT are approximately an order of magnitude smaller than those of the FHAWT. As a result, the helical blade is expected to suffer from less fatigue damage during operation compared to the FHAWT blade. This reduction in fatigue damage is beneficial for the structural reliability, thereby lowering the operation and maintenance costs associated with the turbine. For the FHAWT blade, the maximum deformation occurs under LC2. Once the wind speed exceeds its rated value, the blade pitch controller engages to decrease the blade deformation. Typically, the flapwise deformation is larger than the edgewise deformation since the blade

stiffness in the flapwise direction is smaller. In contrast, there is no significant difference between the tangential and normal deformation on the helical blade. This can be attributed to the inherent structural characteristics of the helical twist angle, as discussed in detail in Deng et al. (2022b).

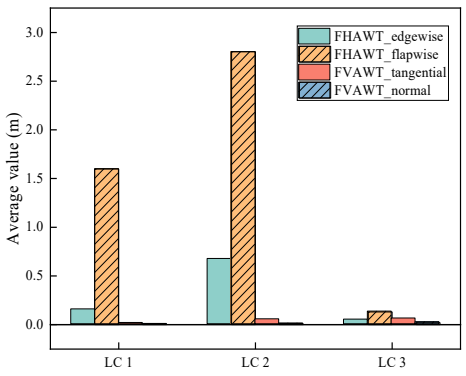

(a) Average value

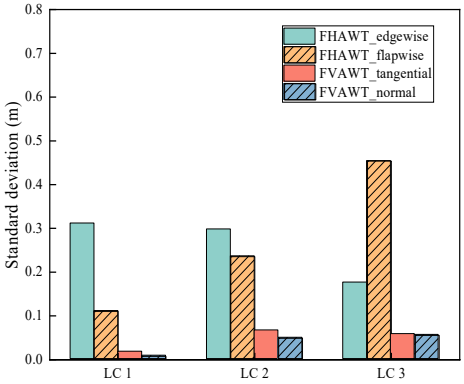

(b) Standard deviation

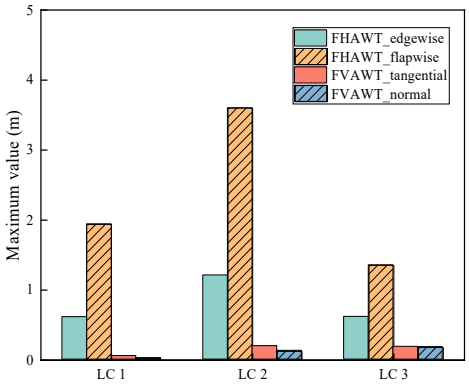

(c) Maximum value

Fig. 18 Statistical results of blade deformations

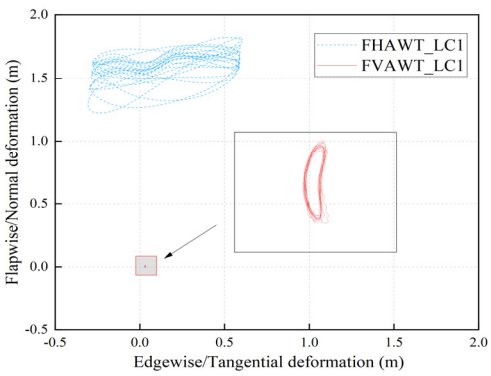

(a) LC 1

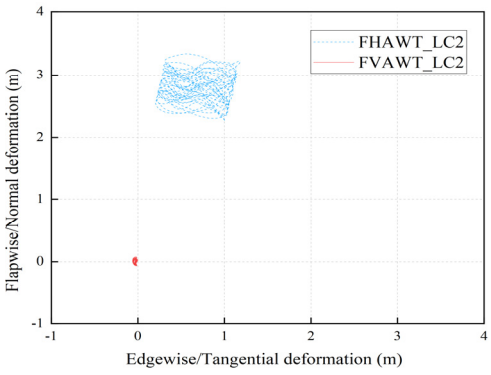

(b) LC 2

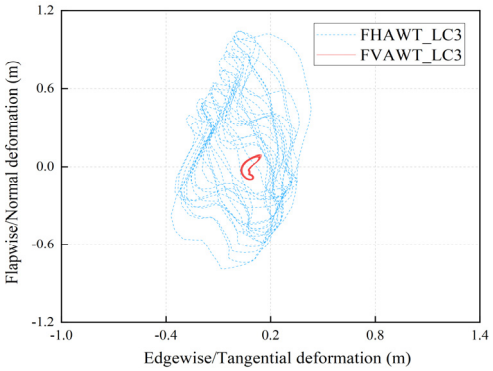

(c) LC 3

Fig. 19 Deformation trajectories of blade deformations

Fourier transform is employed to gain a deeper insight into the dynamic performance of the blades, and the amplitude spectra of the FHAWT blade and FVAWT blade are shown in Figs. 20 and 21. For the FHAWT blade, the frequency components mainly consist of 1P and wave frequency. The 1P frequency exhibits a high peak, demonstrating that the blade deformation is significantly affected by incident aerodynamic loads. For the FVAWT blade, in addition to the 1P and wave frequency, a control frequency is also observed. Moreover, under LC3, multiple aerodynamic frequencies occur on the FVAWT blade, including 1P-4P frequencies.

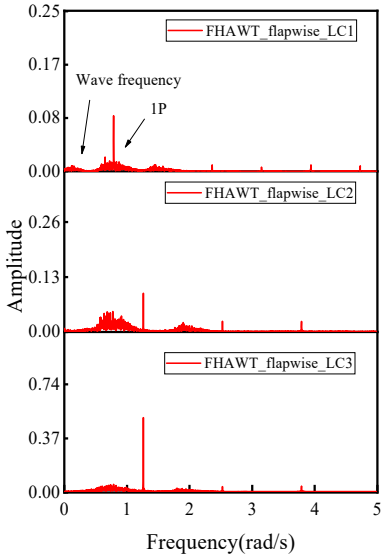

(a) Flapwise deformation

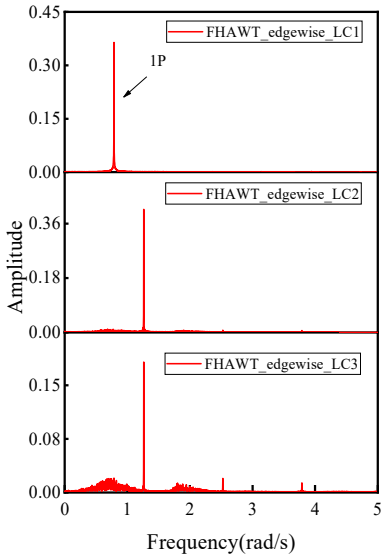

(b) Edgewise deformation

Fig. 20 Amplitude spectra of the FHAWT blade

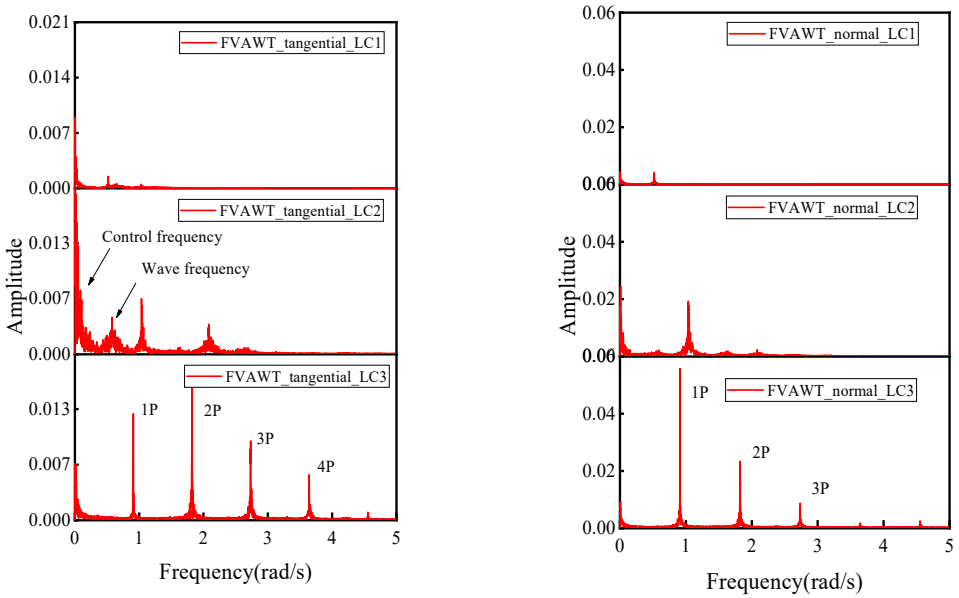

(a) Tangential deformation (b) Normal deformation

Fig. 21 Amplitude spectra of the FVAWT blade

4.6 Blade structural characteristics

Blade deformations are closely related to their structural characteristics. We apply a pulse load on the blade to conduct the free decay simulation and derive the natural frequencies. Table 8 lists the first three order natural frequencies of the FHAWT and FVAWT blade. The FVAWT blade has higher natural frequencies compared to the FHAWT blade. For the FHAWT blade, the first three orders natural frequencies are the 1st flapwise frequency, 1st edgewise frequency, and 2nd flapwise frequency, respectively. In contrast, it is challenging to distinguish the directions of the helical blade frequencies due to the continuous variation in section direction along its length.

Table 8 Natural frequency of the two blades

Item	FHAWT blade (Hz)	Helical blade (Hz)
First order	0.668	2.488
Second order	1.090	3.550
Third order	1.922	4.300

Fig. 22 compares structural parameters of the two blades, including chord length (Chord), mass per length (Mass), tensile stiffness (EA), and bending stiffness in two

directions (EIXX and EIYY). The horizontal axis represents the non-dimensional blade length for comparison purposes. As shown in the figure, the helical blade generally exhibits smaller mass and stiffness.

The analysis above indicates that the FVAWT blade experiences smaller deformations compared to the FHAWT blade although the helical blade has lower section mass and stiffness. This observation can be attributed to two reasons. Firstly, the 120° helical twist angle of the helical blade has been proved to effectively suppress the blade deformation compared to the straight blade (Deng et al., 2022b). Secondly, the FHAWT blade can be considered as a cantilever beam, whist the helical blade can be considered as a three-point fixed beam. Without loss of generality, a cantilever beam is expected to experience greater maximum deformation than a three-point fixed beam under similar conditions.

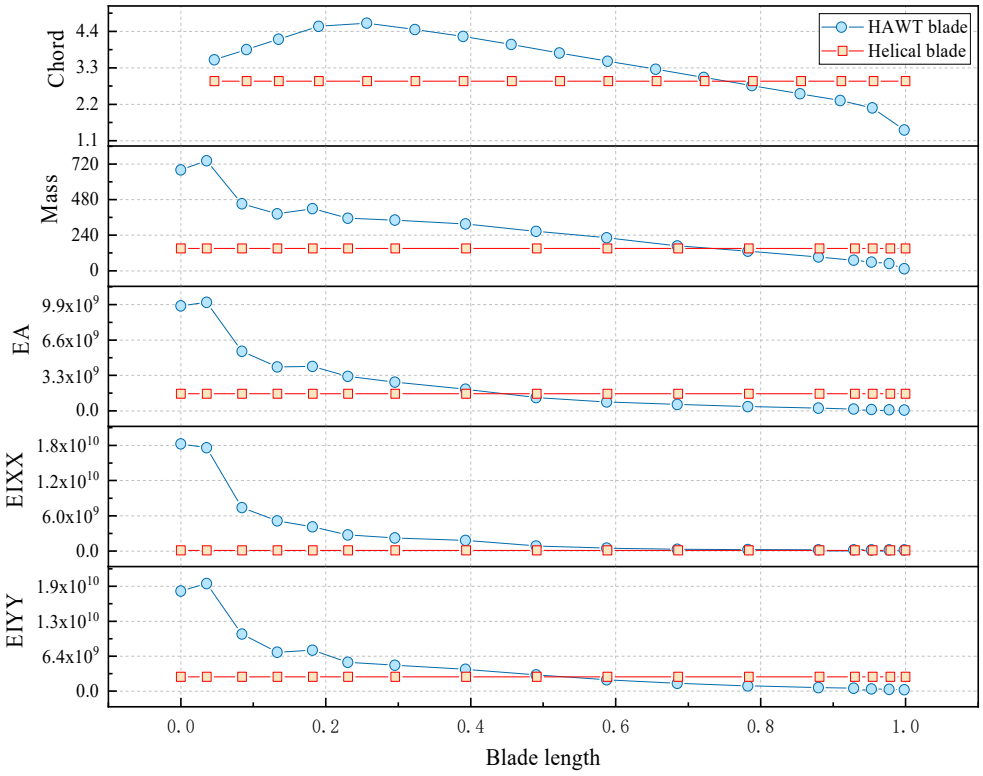

Fig. 22 Structural parameters along the blade

5. Conclusions

Helical type vertical axis floating wind turbines are promising for exploiting wind resources in deep seas. This research conducts a comparative study between a

conventional FHAWT and a helical type FVAWT. Both wind turbines are installed on the same OC4 semi-submersible floating foundation with the same mooring system. The dynamic responses of the helical type FHAWT are calculated using SESAM/Sima software, while dynamic responses of the helical type FVAWT are calculated using our in-house coupled numerical code. A series of code-to-experiment comparisons are conducted to validate the accuracy of the two numerical models, including the free decay test and combined wind and wave test. Afterwards, dynamic characteristics are compared between the FHAWT and helical type FVAWT, focusing on the control strategy, aerodynamic power, floater motions, tower base bending moments, and blade deformations. The following specific conclusions are drawn from this comparative analysis.

(1) The helical type FVAWT has a narrower wind speed working range compared to the FHAWT due to its inferior self-starting performance. In addition, the helical type FVAWT presents higher power fluctuations under all cases. This is attributed to two factors: Firstly, the azimuth angle of the helical type FVAWT blade varies as the rotor rotates, leading to noticeable periodical aerodynamic loads. Secondly, the control strategies are different for the two wind turbines. The FHAWT employs a blade-pitch controller when the wind speed exceeds its rated value. However, the helical blade could not vary its pitch angle, instead only relying on a rotational speed controller, resulting in a larger fluctuation of aerodynamic power.

(2) The floater motions are influenced differently by wind and wave loads. Wave loads mainly affect the amplitude, while wind loads affect the equilibrium position. Therefore, the larger aerodynamic loads on the helical type FVAWT leads to higher mean values of the floater motions than the FHAWT, particularly under LC3. Standard deviations of the two wind turbines have small discrepancy, except for the yaw motion under LC2.

(3) The tower base bending moments for the two wind turbines are primarily dominated by the fore-aft bending components. The helical type FVAWT has lower mean values of fore-aft bending moments than the FHAWT. However, the standard deviations and maximum values of the helical type FVAWT are larger, especially under

LC3. This indicates that a helical type FVAWT tower may suffer from more severe fatigue damage over its lifespan compared to a FHAWT tower.

(4) Despite having lower section mass and stiffness, the helical type FVAWT blade experiences much smaller deformations than the FHAWT blade. This is due to the helical twist angle of the FVAWT blade, which effectively suppresses the blade deformation. In addition, the FHAWT blade can be considered as a cantilever beam, whist the helical type FVAWT blade can be considered as a three-point fixed beam. Typically, the maximum deformation of a cantilever beam is greater than that of a three-point fixed beam under equivalent conditions. Thus, the minimal deformations of the helical type FVAWT blade are favorable for the large-scale trend of the floating wind turbines.

Considering all these aspects, the FHAWT presents the merits on the aerodynamic performance and tower base bending moments. In contrast, the helical type FVAWT has the advantage of minimal blade deformations. Consequently, optimizing the control strategy of the FVAWT is essential for the commercial application. Some novel control strategies have been proposed such as the artificial intelligence algorithm (Poultangari et al., 2012), which is the concern of our subsequent research. In this research, constant wind was considered rather than turbulent wind. This limitation may lead to the underestimation of the low-frequency response of floater motions. Turbulent wind will also affect the power performance of the wind turbine system. In the subsequent work, we intend to conduct more load cases with turbulent wind to further compare the dynamic characteristics of the FHAWT and the helical type FVAWT.

Acknowledgement

This study was supported by the National Natural Science Foundation of China (No.51879190, No.52001230), Natural Science Foundation of Tianjin (No. 21JCQNJC00330), Tianjin Research Innovation Project for Postgraduate Students (No. 2021YJSB185), State Key Laboratory of Alternate Electrical Power System with Renewable Energy Sources (No. LAPS24005). The support provided by China Scholarship Council (CSC No. 202306250078) during a visit of Wanru Deng is

acknowledged.

References

Bangga, G., Dessoky, A., Wu, Z., Rogowski, K., Hansen, M.O.L., 2020. Accuracy and consistency of CFD and engineering models for simulating vertical axis wind turbine loads. Energy, 206, 118087.

https://doi.org/10.1016/j.energy.2020.118087

Battisti, L., Brighenti, A., Benini, E., Castelli, M.R., 2016. Analysis of different blade architectures on small VAWT performance. Journal of Physics: Conference Series 753(6).

https://doi.org/10.1088/1742-6596/753/6/062009

Borg, M., Collu, M., 2015. A comparison between the dynamics of horizontal and vertical axis offshore floating wind turbines. Philosophical Transactions of the Royal Society of London A: Mathematical, Physical and Engineering Sciences, 373(2035), 20140076.

https://doi.org/10.1098/rsta.2014.0076

Cahay, M., Luquiau, E., Smadja, C., Silvert, F., 2011. Use of a vertical wind turbine in an offshore floating wind farm. In: Offshore Technology Conference. Houston, Texas, USA.

https://doi.org/10.4043/21705-MS

Cao, Q., Xiao, L., Cheng, Z., Liu, M., Wen, B., 2020. Operational and extreme responses of a new concept of 10MW semi-submersible wind turbine in intermediate water depth: An experimental study. Ocean Engineering, 217, 108003.

https://doi.org/10.1016/j.oceaneng.2020.108003

Chen, P., Ja, C., Ng, C., Hu, Z., 2021. Application of SADA method on full-scale measurement data for dynamic responses prediction of Hywind floating wind turbines.

Ocean Engineering, 239, 109814.

https://doi.org/10.1016/j.oceaneng.2021.109814

Cheng, Z., Wang, K., Gao, Z., Moan, T., 2017a. A comparative study on dynamic responses of spar-type floating horizontal and vertical axis wind turbines. Wind Energy, 20 (2), 305-323.

http://dx.doi.org/10.1002/we.2007

Cheng, Z., Madsen, H.A., Chai, W., Gao, Z., Moan, T., 2017b. A comparison of extreme structural responses and fatigue damage of semi-submersible type floating horizontal and vertical axis wind turbines. Renewable Energy, 108, 207-219.

https://doi.org/10.1016/j.renene.2017.02.067

Cheng, Z., Madsen, H.A., Gao, Z., Moan, T., 2017c. Effect of the number of blades on the dynamics of floating straight-bladed vertical axis wind turbines. Renewable Energy, 101, 1285–1298.

https://doi.org/10.1016/j.renene.2016.09.074

Deng, W., Gao, X., Liu, L., Zhao, H., 2018. Dynamic Modeling of H-type Floating VAWT considering the Rigid-Flexible Coupling motions. Proceedings of the ASME 37th International Conference on Ocean, Offshore and Arctic Engineering, Madrid, Spain.

https://doi.org/10.1115/OMAE2018-78619

Deng, W., Yu, Y., Liu, L., Guo, Y., Zhao, H., 2020. Research on the dynamical responses of H-type floating VAWT considering the rigid-flexible coupling effect. Journal of Sound and Vibration, 469, 115162.

https://doi.org/10.1016/j.jsv.2019.115162

Deng, W., Liu, L., Li, Y., Zhang, R., Li, H., 2022a. Slack coupled modeling method and dynamic analysis on floating vertical axis wind turbine with helical blades, Ocean Engineering, 246, 110616.

https://doi.org/10.1016/j.oceaneng.2022.110616

Deng, W., Liu, L., Guo, Y., Li, H., 2022b. Effect of helical twist angle on the aerodynamic performance and blade dynamic characteristics of floating vertical axis wind turbines. Marine Structures, 83, 103-172.

https://doi.org/10.1016/j.marstruc.2022.103172

Deng, W., Guo, Y., Liu, L., Li, Y., Jiang, Y., Xie, P., 2023. Dynamic response analysis of a floating vertical axis wind turbine with helical blades based on the model test. Ocean Engineering, 273, 113930.

https://doi.org/10.1016/j.oceaneng.2023.113930

Deng, W., Liu, L., Dai, Y., Wu, H., Yuan, Z., 2024. A prediction method for blade deformations of large-scale FVAWTs using dynamics theory and machine learning techniques. Energy, 304, 132211.

https://doi.org/10.1016/j.energy.2024.132211

Duan, F., Hu, Z., Niedzwecki, J. M., 2016. Model test investigation of a spar floating wind turbine. Marine Structures, 49, 76–96.

https://doi.org/10.1016/j.marstruc.2016.05.011

Equinor, Equinor and ORE Catapult Collaborating to Share Hywind Scotland Operational Data. https://www.equinor.com/en/news/2019-11-28-hywindscotland-data.html/.

Garrad Hassan, G.L., 2012. Bladed User Manual Version 4.2. Garrad Hassan&Partners Ltd, St Vincent's Works, Bristol, England.

Goupee, A. J., Koo, B., Kimball, R. W., Lambrakos, K. F., Dagher, H. J., 2012. Experimental Comparison of three floating wind turbine concepts. In: Proceedings of the 31st International Conference Offshore Mechanics and Arctic Engineering, Rio de Janeiro, Brazil.

https://doi.org/10.1115/omae2012-83645

Guo, Y., Liu, L., Lv, X., Tang, Y., 2019. The aerodynamic analysis of helical-type VAWT with semi empirical and CFD method. In: ASME 38th international conference on ocean. Glasgow, Scotland, UK: Offshore and Arctic Engineering.

https://doi.org/10.1115/OMAE2019-95207

Hand, B., Cashman, A., 2020. A review on the historical development of the lift-type vertical axis wind turbine: From onshore to offshore floating application. Sustainable Energy Technologies and Assessments, 38, 100646.

https://doi.org/10.1016/j.seta.2020.100646

Hansen, J.T., Mahak, M., Tzanakis, L., 2021. Numerical modelling and optimization of vertical axis wind turbine pairs: a scale up approach. Renewable Energy, 171, 1371–81.

https://doi.org/10.1016/j.renene.2021.03.001

Hanson, T., Skaare, B., Yttervik, R., Nielsen, F., Havmoller, O., 2011. Comparison of Measured and Simulated Responses at the First Full Scale Floating Wind Turbine HYWIND, Tech. Rep., EWEA OFFSHORE.

Jiang, Y., Liu, S., Zao, P., Yu, Y., Zou, L., Liu, L., Li, J., 2022. Experimental evaluation of a tree-shaped quad-rotor wind turbine on power output controllability and survival shutdown capability. Applied Energy, 309, 118350.

https://doi.org/10.1016/j.apenergy.2021.118350

Jing, L., Htet, L., Jun, Z., 2019. Review on the technical perspectives and commercial viability of vertical axis wind turbines. Ocean Engineering, 182(15), 608-626.

https://doi.org/10.1016/j.oceaneng.2019.04.086

Johannessen, K., Meling, T. S., Haver, S., 2002. Joint distribution for wind and waves in the northern north sea. International Journal of Offshore and Polar Engineering, 12 (1).

Jonkman, J., Marshall, L., Buhl, J.R., 2005. FAST User's Guide-updated August 2005. No. NREL/TP-500e38230, National Renewable Energy Laboratory (NREL), Golden,

CO.

Jonkman, J., Butterfield, S., Musial, W., Scott, G., 2009. Definition of a 5-MW Reference Wind Turbine for Offshore System Development. Technical Report, National Renewable Energy Laboratory, Golden, CO. No. NREL/TP-500e38060.

Kuang, L., Lu Q., Huang, X., Song, L., Chen, Y., Su, J., Han, Z., Zhou, D., Zhao, Y., Xu, Y., Liu, Y., 2022. Characterization of wake interference between two tandem offshore floating vertical-axis wind turbines: Effect of platform pitch motion. Energy Conversion and Management, 265, 115769.

https://doi.org/10.1016/j.enconman.2022.115769

Leonardo, D., Biswajit, B., 2008. Unavailability of wind turbines due to wind-induced accelerations. Engineering Structures, 30(4), 885-893.

https://doi.org/10.1016/j.engstruct.2007.05.015

Li, Y., Zhu, Q., Liu, L., Tang, Y., 2018. Transient response of a SPAR-type floating offshore wind turbine with fractured mooring lines. Renewable Energy, 122, 576–588.

https://doi.org/10.1016/j.renene.2018.01.067

Li, Y., Liu, L., Guo, Y., Deng, W., 2022. Numerical Prediction on the Dynamic Response of a Helical Floating Vertical Axis Wind Turbine Based on an Aero-Hydro-Mooring-Control Coupled Model. Energies, 15, 3726.

Li, Y., Li, H., Wang, Z., Li, Y., Wang, B., Tang, Y., 2023. The dynamic response of a Spar-type floating wind turbine under freak waves with different properties. Marine Structures, 91, 103471.

https://doi.org/10.1016/j.marstruc.2023.103471

Li, Y., Li, H., Wang, B., Meng, H., Su, O., Tang, Y., 2024a. Effects of various freak waves on dynamic responses of a Spar-buoy floating offshore wind turbine. Ocean Engineering, 311, 118837.

https://doi.org/10.1016/j.oceaneng.2024.118837

Li, H., Li, Y., Li, G., Zhu, Q., Wang, B., Tang, Y., 2024b. Transient tower and blade deformations of a Spar-type floating wind turbine in freak waves. Ocean Engineering, 294, 116801.

https://doi.org/10.1016/j.oceaneng.2024.116801

Liu, L., Guo, Y., Zhao, H., Tang, Y., 2017. Motions of a 5 MW floating VAWT evaluated by numerical simulations and model tests. Ocean Engineering, 144, 21-34.

https://doi.org/10.1016/j.oceaneng.2017.08.004

Molins, C., Trubat, P., Gironella, X., Campos, A., 2015. Design optimization for a truncated catenary mooring system for scale model test. Journal of Marine Science and Engineering, 3 (4), 1362–1381.

https://doi.org/10.3390/jmse3041362

Nakamura, T., Mizumukai, K., Akimoto, H., Hara, Y., Kawamura, T., 2013. Floating axis wind and water turbine for high utilization of sea surface area-design of sub-megawatt prototype turbine. Proceedings of the ASME 2013 32nd International Conference on Ocean, Offshore and Arctic Engineering, Nantes, France. p. 1–6.

https://doi.org/10.1115/OMAE2013-11287

Nielsen, F.G., Hanson, T.D., Skaare, B., 2006. Integrated dynamic analysis of floating offshore wind turbines. In: Proceedings of the 25th International Conference Offshore Mechanics and Arctic Engineering, Hamburg, Germany.

https://doi.org/10.1115/omae2006-92291

Ormberg, H., Bachynski, E.E., 2012. Global Analysis of Floating Wind Turbines: Code Development, Model Sensitivity and Benchmark Study. Proceedings of the Twenty-second International Offshore and Polar Engineering Conference, Rhodes, Greece.

Paulsen, U. S., Borg, M., H. Madsen, A., Pedersen, T. F., Hattel, J., Ritchie, E., Ferreira, C. S., Svendsen, H., Berthelsen, P. A., Smadja, C., 2015. Outcomes of the deepwind conceptual design. Energy Procedia, 80, 329–341.

https://doi.org/10.1016/j.egypro.2015.11.437

Poultangari, I., Shahnazi, R., Sheikhan, M., 2012. RBF neural network based PI pitch controller for a class of 5-MW wind turbines using particle swarm optimization algorithm, ISA transactions 51(5), 641.

https://doi.org/10.1016/j.isatra.2012.06.001

Qu, X., Li, Y., Tang, Y., Hu, Z., Zhang, P., Yin, T., 2020. Dynamic response of spar-type floating offshore wind turbine in freak wave considering the wave-current interaction effect. Applied Ocean Research, 100, 102178.

https://doi.org/10.1016/j.apor.2020.102178

Ractliffe, A.T., 1985. The validity of quasi-static and approximate formulae in the context of cable and flexible riser dynamics. 4th International Conference on Behaviour of Offshore Structures, Delft, The Netherlands.

https://trid.trb.org/view/42803

RIFLEX 4.14.0 User Guide, 2018.

Robertson, A., Jonkman, J., Masciola, M., Song, H., Goupee, A., Coulling, A., Luan, C., 2012. Definition of the Semisubmersible Floating System for Phase II of OC4. Offshore Code Comparison Collaboration Continuation (OC4) for IEA Task 30.

Roddier, D., Cermelli, C., Aubault, A., Weinstein, A., 2010. WindFloat: A floating foundation for offshore wind turbines. Journal of Renewable and Sustainable Energy, 2(3), 033104.

https://doi.org/10.1063/1.3435339

SeaTwirl AB. Available online: https://seatwirl.com/.

SIMO 4.14.0 User Guide, 2018.

Simone, G., Giulio, P., Stefania, Z., 2015. CFD investigation on the aerodynamic interferences between medium-solidity Darrieus Vertical Axis Wind Turbines. Energy Proc, 81, 227–39.

https://doi.org/10.1016/j.egypro.2015.12.089

Stehly, T., Beiter, P., Duffy, P., 2019. Cost of Wind Energy Review. National Renewable Energy Laboratory.

The world's most powerful available wind turbine gets major power boost, 2017.

http://www.mhivestasoffshore.com/worlds-most-powerful-available-wind-turbine-gets-major-power-boost/.

V117-4.2 MW™ at a glance, 2010.

https://www.vestas.com/en/products/4-mw-platform/v117-4_2_mw#

Wang, K., Moan, T., Hansen, M.O.L., 2013. A method for modeling of floating vertical axis wind turbine. Proceedings of the 32th International Conference on Ocean, Offshore and Arctic Engineering, Nantes, France.

https://doi.org/10.1115/OMAE2013-10289

Wang, K., Luan, C., Moan, T., Hansen, M.O.L., 2014. Comparative study of a FVAWT and a FHAWT with a semi-submersible floater. Proceedings of the 24th International Ocean and Polar Engineering Conference, Busan, South Korea.

Xu, J., L. Zhang, X. Li, S. Li, K. Yang, 2020. A study of dynamic response of a wind turbine blade based on the multi-body dynamics method. Renewable Energy, 155, 358-368.

https://doi.org/10.1016/j.renene.2020.03.103

Zhang, D., Wu Z., Chen, Y., Kuang, L., Peng, Y., Zhou, D., Tu Y., 2024. Full-scale vs. scaled aerodynamics of 5-MW offshore VAWTs under pitch motion: A numerical analysis. Applied Energy, 372, 123822.

https://doi.org/10.1016/j.apenergy.2024.123822

Zhang, L., Li, Y., Xu, W., Gao, Z., Fang, L., Li, R., Ding, B., Zhao, B., Leng, J., He, F., 2022. Systematic analysis of performance and cost of two floating offshore wind

turbines with significant interactions. Applied Energy, 321(1), 119341. https://doi.org/10.1016/j.apenergy.2022.119341